
Article:
Robertson, Ben, Thompson, Richard L., McLeish, Tom C.B. orcid.org/0000-0002-2025-0299 et al. (1 more author) (2019) Polymer extrudate-swell : From monodisperse melts to polydispersity and flow-induced reduction in monomer friction. Journal of Rheology. pp. 319-333. ISSN 1520-8516

https://doi.org/10.1122/1.5058207

Polymer extrudate-swell: From monodisperse melts to polydispersity and flow-induced reduction in monomer friction

Ben Robertson, Richard L. Thompson, Tom C. B. McLeish, and Ian Robinson

Citation: Journal of Rheology **63**, 319 (2019); doi: 10.1122/1.5058207
View online: https://doi.org/10.1122/1.5058207
View Table of Contents: https://sor.scitation.org/toc/jor/63/2
Published by the The Society of Rheology

Polymer extrudate-swell: From monodisperse melts to polydispersity and flow-induced reduction in monomer friction

Ben Robertson,[1,a)] Richard L. Thompson,[1] Tom C. B. McLeish,[2] and Ian Robinson[3]

[1]*Department of Chemistry, Durham University, Durham DH1 3LE, United Kingdom*
[2]*Department of Physics, University of York, York YO10 5DD, United Kingdom*
[3]*Lucite International, Wilton, Redcar TS10 4RF, United Kingdom*

(Received 18 September 2018; final revision received 6 February 2019; published 26 February 2019)

Abstract

This paper describes finite-element simulations and associated experimental studies of extrudate swell for near-monodisperse and polydisperse polystyrenes. The tube-model based Rolie-Poly constitutive model, when extended to include a reduction of monomeric friction at high extension rates, makes much-improved predictions of extrudate swell at high Weissenberg number. This is especially significant for near-monodisperse polymers where rheological features are unchanged by the effects of polydispersity. Extension of this molecular rheology scheme to a polydisperse constitutive model addresses extrusion experiments on polydisperse polystyrenes inside a multipass rheometer, accounting for experimental data up to Rouse Weissenberg numbers of 50. We, therefore, show that from a measurement of polymer molecular weight distribution, it is possible to predict extrudate swell over a broad range of processing conditions for polydisperse polymers and realistic extrusion processes. Small changes in the capillary length to diameter ratio have little effect on extrudate swell in this range of Weissenberg number. This is because the capillary residence time is sufficiently long for a steady state to be reached within the polymer stretch relaxation time, which controls the most decisive physics responsible for extrudate swell. https://doi.org/10.1122/1.5058207

I. INTRODUCTION

The vast majority of previous work on extrudate swell directly addresses systems of industrial complexity. Commercial polydisperse, crystalline, polymer melts in nonisothermal extrusion exhibit swelling strongly controlled by crystallization [1], as well as very complex molecular interactions. Useful trends can be identified, but a fully predictive theory has not emerged. The advent of molecular rheological theories based on entanglement models has opened up the possibility of a fully molecular, multiscale, and predictive approach to complex flow phenomena in polymer melts, such as extrudate swell. The aim of the longer program within which this work constitutes a stage is to provide such a method for predicting extrudate swell, from arbitrary die geometries, and eventually for industrially relevant polydisperse polymers, by using approximately monodisperse polymers [2], and then building up in complexity by addressing bidisperse and polydisperse polymers (this work). In future work, we will apply these simulations to branched systems to show that tube-model based theories can be used to predict a wide number of industrial polymers in relevant flow geometries.

A. Extrudate swell

Extrudate swell is a longstanding industrial problem and is only just receiving theoretical analysis using a molecular theory [2]. Until recently, it has only been approximately predicted using phenomenological approaches based on correlations of observed swell with rheometric characteristics, especially the dependence on normal stress difference [3,4], and die entry pressure drops [5,6]. None of these studies adequately provides a molecular basis for their predictions or differences observed between predictions and experiments. Some previous studies have investigated the effect of polydispersity on extrudate swell. For example, *Den-Doelder* and *Koopmans* investigated the effect of molecular weight distribution upon extrudate swell on a series of polyethylene melts [7]. They found a general increase in extrudate swell with increasing weight average molecular weight, although dispersity also had a significant effect. Indeed, at high molecular weights, a decrease in swelling with increasing average molecular weight was seen in some cases, when accompanied by a decrease in dispersity. Dispersity was not the only relevant parameter; the higher moments of the molecular mass distribution were also important. They concluded that a high molecular weight tail has a very significant effect on the extrudate swell, although they did not explain this on a molecular level through a tube theory based model or otherwise.

It is useful to understand extrudate swell in monodisperse melts before attempting to understand it in these more complex molecular weight distributions. An introduction to extrudate swell for monodisperse polymer melts can be found in [2] and is summarized in Sec. I B.

B. Monodisperse simulations

The two main tools we use to simulate our polymer flows are the tube-model based Rolie-Poly (Rouse Linear Entangled Polymer) model [8] for nonlinear response and the

[a)]Author to whom correspondence should be addressed; electronic mail: ben.robertson@dunelm.org.uk

formulation of linear theory for entangled polymer melts of Likhtman–McLeish [9]. This theory is used to model the rheology of linear, monodisperse polymers. It can fit the linear rheology of an entangled polymer melt and extract the Rouse relaxation time τ_R and the reptation relaxation time, τ_d

$$\tau_d = 3\tau_e Z^3\left(1 - \frac{3.38}{\sqrt{Z}} + \frac{4.17}{Z} - \frac{1.55}{Z^{3/2}}\right), \qquad \tau_R = \tau_e Z^2. \tag{1}$$

$Z = M_w/M_e$, the number of entanglements per chain, where M_w is the weight average molecular weight of the chain and M_e is the molecular weight of one entanglement segment. τ_e is defined as the Rouse relaxation time of one entanglement segment.

To extend the tube model to strongly nonlinear flows requires a stochastic partial differential structure (the Graham, Likhtman and Milner-McLeish or GLAMM model [10]) in the form of an ordinary tensorial differential equation. The GLAMM model carries sufficient variables to calculate in a preaveraged approximation, both the stress and the structure factor of a monodisperse polymer melt. The Rolie-Poly [8] constitutive equation is a single mode simplification of this model, helpful when only the stress is required, and much faster to calculate with. It is currently required for finite-element calculations of complex flows. A series of "Rolie-Poly elements," each assigned to a relaxation modulus, reptation time, and Rouse relaxation time, are taken as inputs to the model and summed up to give overall polymeric stress. For the monodisperse simulations, the higher frequency elements represent different interior relaxation modes of the "monodisperse" chain. These interior modes are noninteracting and thus are calculated separately and then summed.

There are two types of element in the summed model: for low frequency elements, for which chain-stretching occurs within the simulation time scale, the relevant form of the time-development of stress, $\boldsymbol{\sigma}$ is given by

$$\frac{d\mathbf{A}}{dt} = \boldsymbol{\kappa}\cdot\mathbf{A} + \mathbf{A}\cdot\boldsymbol{\kappa}^T - \frac{1}{\tau_d}(\mathbf{A} - \lambda^2\mathbf{I}) - \frac{2}{\tau_R}\left(F(\lambda) - \frac{1}{\lambda}\right)\mathbf{A} - \frac{2\beta}{\tau_R}\left(F(\lambda) - \frac{1}{\lambda}\right)\frac{F(\lambda)}{\lambda}\left(\mathbf{A} - \frac{1}{F(\lambda)}\mathbf{I}\right),$$

where

$$F(\lambda) = \left(\frac{\lambda_{\max}^2 - \lambda^2/3}{\lambda_{\max}^2 - \lambda^2}\right)\left(\frac{\lambda_{\max}^2 - 1}{\lambda_{\max}^2 - 1/3}\right), \qquad \boldsymbol{\sigma} = GF(\lambda)\mathbf{A}. \tag{2}$$

The finite extensibility function $F(\lambda)$ is the *Padé* approximant to the inverse Langevin function, $\boldsymbol{\kappa}$ is the velocity gradient tensor, $\boldsymbol{\sigma}$ is the polymeric stress tensor, $\mathbf{A}$ is the auxiliary tensor describing the chain configuration, $\mathbf{I}$ is the identity matrix, β is a parameter describing the level of constraint release, λ is the chain stretch, calculated using the equation $\lambda = \sqrt{(\text{trace}(\mathrm{A})/3)}$, and $\lambda_{\max}$ is the finite extensibility of chains. This value, $\lambda_{\max}$, defines the maximum extension that can theoretically be applied to a chain, i.e., when the chain dimension equals its contour length. The Rouse time, reptation time, and modulus for each Rolie-Poly element are given by τ_R, τ_d, and G, respectively. This finite extensibility equation is used as it is the form previously incorporated in the *RepTate* and *flowSolve* software packages used in this work.

For high frequency elements, which are nonstretching at all flow rates in a simulation, the nonlinearity arising from chain stretch can be removed from the dynamical equation to give a simplified form for the auxiliary tensor $\mathbf{A}$

$$\frac{d\mathbf{A}}{dt} = \boldsymbol{\kappa}\cdot\mathbf{A} + \mathbf{A}\cdot\boldsymbol{\kappa}^T - \frac{1}{\tau_d}(\mathbf{A} - \mathbf{I}) - \frac{2}{3}\text{trace}(\boldsymbol{\kappa}\cdot\mathbf{A})(\mathbf{A} + \beta(\mathbf{A} - \mathbf{I})). \tag{3}$$

In this case, the contribution of each element to the polymeric stress is simply the auxiliary tensor multiplied by the modulus of the element. The Rouse relaxation terms in the full equation are replaced in Eq. (3) by a single constraint release term, whereas the reptation relaxation term and flow terms are unmodified.

In our previous work [2], we predicted extrudate swell using the Rolie-Poly equation and compared the predictions to isothermal extrudate swell experiments within a modified multipass rheometer (MPR). We found that at a constant apparent wall shear rate, the extrudate swell (characterized by a dimensionless ratio of extrudate width to capillary diameter, the "B value") increased with increasing molecular weight. When the shear rate is made dimensionless by the chains' Rouse time, so forming a "Rouse Weissenberg number," the extrudate swell as a function of flow rate from samples with different molecular weights collapses onto a single curve. We define the Rouse Weissenberg number as

$$W_R = \dot{\gamma}_w \tau_R, \tag{4}$$

where $\dot{\gamma}_w$ is the apparent (Newtonian) wall shear rate and τ_R is, as usual, the Rouse relaxation time of the polymer. We also found an agreement between experimental and simulated B values for $W_R < 7$, including the predicted data-collapse with W_R. Above this point, the data from the MPR show a reduction in the gradient of the increase of extrudate swell with shear rate, relative to the theoretical predictions. We hypothesized but did not investigate in that work that this may be due to a reduction in the monomeric friction coefficient at these high shear rates, as such effects had been previously implicated in extensional flows of monodisperse polystyrenes under uniaxial extension [11,12] but have not previously been considered for extrusion processes.

We also measured extrudate swell experiments for a bidisperse polymer melt. This melt behaved differently to the monodisperse case, showing larger swelling at low shear rates than that predicted by a monodisperse melt of the same mean molecular weight. This swelling was consistent with the higher molecular weight component in the blend having an inflated Rouse time, caused by dilution with the short chains and enhancing the crucial chain stretch [13]. This is discussed in Sec. I D.

C. Friction reduction

The tube theory used thus far assumes that the relaxation time scales of polymer chains under fast flow are the same as the time scales under slow flow. Recently, however, evidence

has been found that this is not the case and that relaxation is accelerated under fast flow. In [11], this was thought to be due to monomeric friction reduction and in [14] due to flow induced disentanglement. In our calculations, we focus on monomeric friction reduction, but we note that both effects will reduce relaxation times at high Weissenberg number. In this work, we have introduced an important modification to the physics of molecular friction reduction, so next we briefly review work on modeling it to date.

The value of monomeric friction reduces because the increasing chain alignment that occurs at high shear rates eventually induces an anisotropy in the local environment of monomers. At sufficiently high rates, the Kuhn segments orient significantly in the flow direction, exerting a smaller frictional force upon similarly aligned and adjacent Kuhn segments. Neighboring chains are thus able to move past each other more freely than if they were in a random orientation. This lower friction results in a lowering of the relaxation time of an entanglement segment, τ_e, and thus the Rouse and reptation relaxation times.

Yaoita *et al.* [12] performed simulations of polystyrene melts under extensional flows. This chemistry shows the greatest effects in studies of monomeric friction reduction because of polystyrene's low finite extensibility coefficient $\lambda_{\max}$. This ensures that reduced friction constants are reached at relatively low rates. Yaoita *et al.* replaced the constant friction in their rheological model with a variable friction which is a function of a stretch-orientation factor, F_{SO}. They fitted the extensional flow data to an empirical form and found that there was a lower critical value of F_{SO} of 0.14 above which the friction reduction began. Yaoita *et al.* used this fitted parameter within Primitive Chain Network simulations, incorporating these friction reduction equations. They found that without the reduction, the simulations overpredicted start-up extensional viscosities but gave good agreement when it is included. The effect is especially visible for higher molecular weight polystyrenes where the extension hardening is significant. Furthermore, friction reduction was found to cause only small changes in the start-up extensional viscosities under uniaxial extension, the major effect was in the steady-state prediction. Steady-state viscosity predicted by the unmodified model was too high but friction reduction allowed the model to approximately match the plateau observed in the data. Friction reduction had no effect on a low molecular weight polymer or at low extension rates where the predictions matched data without friction reduction. It also had no effect on the transient shear predictions even at high shear rates.

Ianniruberto [15], in an alternative model, kept the critical order parameter but replaced the mathematical form used by Yaoita *et al.* [12] with a much simpler power law form. For stretching parallel to the flow direction, this reads

$$\begin{aligned}\zeta &= (S/S_c)^{-1.25}: S \geq S_c,\\ \zeta &= 1: S < S_c,\\ S &= \left(\frac{\bar{\lambda}}{\lambda_{\max}}\right)^2 (\bar{S}_{xx} - \bar{S}_{yy}),\end{aligned} \tag{5}$$

where ζ is the monomeric friction reduction coefficient, defined as $\zeta(S)/\zeta_0$, the ratio of monomeric friction at a specific orientation over the equilibrium monomeric friction. At slow deformation rates, the friction reduction coefficient will be 1 and the friction will have the value of ζ_0. The over bar quantities indicate averages over all chains. S_{xx} and S_{yy} describe the xx and yy components, respectively, of the orientation tensor $\mathbf{S}$. This orientation is related to the Rolie-Poly conformation tensor $\mathbf{A}$ via $\mathbf{S} = (\mathbf{A}/\mathrm{trace}(\mathbf{A}))$.

Ianniruberto *et al.* also performed molecular dynamics on oligomers to simulate polymers under extensional flow [11]. They measured the diffusion coefficient of a test chain at different levels of monomer alignment and thus related this to the monomeric friction. They also found a switch-on in monomeric friction reduction at a critical value, 0.063, of Kuhn segment alignment.

This basic power S^{-n} form has also been used by Mead *et al.* in [16], as well as in [17,18], for polydisperse melts in which they used a -1.64 power law and replaced the single S_{Kuhn} by an orientation factor S_i for each weight fraction of chain, i

$$S_i = \sqrt{S_{\mathrm{Kuhn},i} \cdot \sum_j \phi_j S_{\mathrm{Kuhn},j}}, \tag{6}$$

where ϕ_j is the weight fraction of chains j in the melt. The theory was based upon slip-link methods rather than the pure tube theory approach discussed here.

In this work, we will continue to use differential representations of the tube model rather than slip-link schemes, as this permits the simulation of complex flow fields much more readily, though in the spirit of Mead *et al.* recognize the complex interaction between components in a polydisperse blend under strong flows.

The Rouse and reptation times are assumed to be directly proportional to the magnitude of the monomeric friction coefficient at all rates.

In the present study, we use the basic form of Yaoita *et al.* from Eq. (5) to calculate ζ, although we add a new element: a minimum friction term $\zeta_{\min}$ to avoid the monomeric friction unphysically reducing to 0 at high extension rates (e.g., at the exit of the extrusion die). $\zeta_{\min}$ represents the value of monomer friction in a completely oriented local environment. Our model can be written as

$$\begin{aligned}\zeta &= \zeta_{\min} + (1 - \zeta_{\min})(S/S_c)^{-1.25}: S \geq S_c,\\ \zeta &= 1: S < S_c.\end{aligned} \tag{7}$$

The order parameter S is calculated from the overall chain orientation of all Rolie-Poly elements in a simulation via

$$\begin{aligned}S &= \frac{\lambda^2}{\lambda_{\max}^2}(\bar{S}_{xx} - \bar{S}_{yy}): \bar{S}_{xx} > \bar{S}_{yy},\\ S &= \frac{\lambda^2}{\lambda_{\max}^2}(\bar{S}_{yy} - \bar{S}_{xx}): \bar{S}_{yy} > \bar{S}_{xx},\\ \bar{\mathbf{S}} &= \frac{\sum_{i=1}^{N_{\mathrm{modes}}} \mathbf{A}_i/\mathrm{trace}(\mathbf{A}_i)}{N_{\mathrm{modes}}},\end{aligned} \tag{8}$$

where N_{modes} is the number of Rolie-Poly elements in the simulation, excluding any high frequency elements which are

modeled as solvent for the purposes of the simulation [19]. $\mathbf{A}_i$ is the Rolie-Poly configuration tensor for each element, and $\bar{\mathbf{S}}$ is the overall orientation tensor normalized to unit trace. The tensor $\mathbf{S}$ and thus the friction reduction and relaxation time terms are all recalculated at each timestep of the simulation, resulting in varying relaxation times throughout the simulation run.

This model gives a single, isotropic friction reduction term for relaxation in the two simulation dimensions. It may be necessary in future to consider an anisotropic friction reduction tensor which would allow for faster relaxation of stress in the flow direction but not against it. This is not performed in our finite-element simulations, however (see Sec. III A), equivalent to the assumption that orientation in a specific triangle is solely in either the *xx* or *yy* directions.

D. Bidisperse and polydisperse theories

The Rolie-Poly constitutive equation, as currently formulated, does not include the change in the relaxation times of polymer chains due to constraint release between different weight fractions when used in multimode form as a model of blends [13]. Although reasonable fits to experimental data can be obtained by introducing multiple stretch times across the spectrum of modes, we require a more fundamental approach here. To complete the program of a predictive scheme taking molecular weight distribution and process conditions as an input, and predicting the extrudate swell, requires an approach that can extract relaxation times from knowledge of the molecular structure and the molecular weight distribution of the blend without empirical fitting.

An early theory for polydisperse systems that does contain a mutual effect on (reptation) relaxation times is "double reptation." This approach describes a polymer melt as a series of binary entanglements between two chains, *s* and *l*. Given that either of the two chains can reptate to relieve the entanglement, the stress σ at time t is proportional to the square of the total tube survival probability $P(t)$ summed over all chains

$$\sigma(t) = G_N^0 P(t)^2, \tag{9}$$

where G_N^0 is the plateau modulus of the material. At the simplest level of approximation, the mean tube survival probability can be calculated to be a weighted sum of the single-exponential Maxwell relaxations of the individual components which in the case of the bimodal blend reads [20]

$$P(t) = \phi_s e^{-t/\tau_{d,s}} + \phi_l e^{-t/\tau_{d,l}}, \tag{10}$$

where ϕ_s is the volume fraction of short chains in a sample and $\phi_l = 1 - \phi_s$ is the volume fraction of long chains. $\tau_{d,s}$ is the reptation time of short chains, and $\tau_{d,l}$ is the reptation time of long chains. This single-exponential approximation incorrectly predicts the shape of the peaks in a linear viscoelastic G'' vs frequency plot, overestimating their sharpness in the case of strictly bimodal blends. The single-exponential form of Eq. (10) can, however, be replaced with a spectrum of relaxation times. For polydisperse rather than bidisperse systems, the stress can be calculated within the double reptation approximation by summing up the survival probabilities of all molecular weight components, *i*

$$\sigma(t) = G_N^0 \left(\sum_i \phi_i P(t, i) \right)^2, \tag{11}$$

where ϕ_i is the volume fraction of *i* chains. This multimode double reptation method produces reasonable results when predicting the linear viscoelastic response of continuously distributed polymers, including the materials used in this study. To address phenomena such as extrudate swell, however, which depend on extension hardening, in a polydisperse linear blend, requires a method in the same spirit but addressing the nonlinear process of stretch relaxation as well as the linear relaxation due to reptation. The method we use here is that of Boudara *et al.* [21,22], the underlying physics of which is discussed below.

In a pure bidisperse blend of long chains *l* and short chains *s*, a test chain *l* is entangled not only with other *l* chains but also with short chains. Within the tube model, we think of the chain being constrained within two tubes as described in Fig. 1:

- A "fat" tube formed by long chains only.
- A "thin" tube formed by all chains in the melt.

The test chain can relax via reptation along the thin tube, by constraint release and contour length fluctuations of the thin tube but also by reptation of the thin tube along the fat tube. This leads to various possible limiting relaxation rates, depending upon the ratios of individual chain relaxation times. Read *et al.* [23] describe a modified "Viovy" diagram [24], where the different relaxation mechanisms of long and short chains are separated out graphically in regimes of different dimensionless parameters. A region of particular interest is that in which contour length fluctuations in the fat tube cause an acceleration of relaxation of the long chains. In this regime, simple double reptation will fail and a more sophisticated picture of chain relaxation is needed. Read *et al.* separated out regions where one would expect stretch time enhancement of long chains by shorter chains in terms of the relative number of entanglements on each chain. Crucially, the polydisperse Rolie-Double-Poly (RDP) equation set used in this work accounts for these different cases and applies relaxation time enhancement where it would be expected to occur from an understanding of the physics.

Auhl *et al.* show how this method of describing a blend leads to the counterintuitive result that the stretch relaxation time of a long chain ($\tau_{R,l}$) within a blend of short chains is

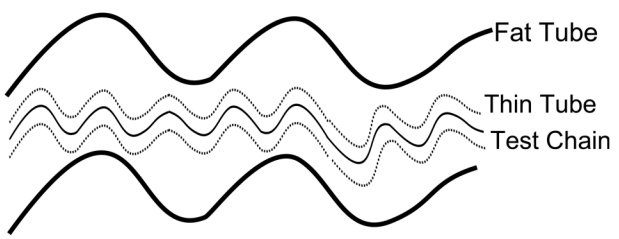

FIG. 1. Schematic diagram of the concept of a chain contained within two tubes.

increased by the inverse of its volume fraction ϕ_l [13]

$$\tau_{R,l} = \frac{\tau_R}{\phi_l}. \tag{12}$$

This leads to the result that, as a melt of long chains is diluted by short chains, the stretch time of the long chains increases the more diluted the chains are. In our previous work, we found that using this formula to increase the Rouse time of the long chains in a bidisperse blend produced an improved fit to extrudate swell data at low shear rates.

Read *et al.* [25] developed a model for bidisperse blends, incorporating several mechanisms for relaxation within both fat and thin tubes. The rates for constraint release, reptation, and stretch relaxation in each tube relative to the deformation rate are considered. They calculate these for the linear rheology of several polystyrene blends and match the nonlinear rheology using very few fitting parameters. In particular, the model correctly predicted the onset of extension hardening at low strain rates. Some overestimations in extensional viscosity were observed at high shear rates. We are most interested here in the agreement at low shear rates, especially in the potential prediction of the abnormally large extrudate swell at low average Weissenberg numbers.

The generalization of this approach to continuous polydispersity by Boudara [21] incorporated the physics of the model into a mode-coupled Rolie-Poly model for blends theory, later called RDP. As usual, the total stress tensor, $\boldsymbol{\sigma}$, is calculated by adding up the stress over a series of Rolie-Poly elements. Boudara compared the predictions of the RDP model to start-up shear and extension experiments on polydisperse polystyrenes and found a reasonable agreement in extensional flow. In the case of bidisperse polyisoprenes, shear viscosities were overestimated by the bidisperse RDP theory at high rates in start-up shear, however, indicating that further work is required in this theory. We describe the equations of motion for all components fully in the Appendix.

The multimode formalism for the RDP theory contains a new set of elements which differs conceptually from the "multimode Rolie-Poly" model of a monodisperse melt. In the latter case, the high frequency elements represent uncoupled internal relaxation modes of the monodisperse chain. The highest frequency of these chain fluctuations is used to form a solvent term for flow simulation. For the RDP model of a polydisperse blend, high frequency elements represent the way that the relaxation of fundamental modes of lower molecular weight chains couple with all other chains in the melt. In the most extreme example, the shortest chains may constitute effective "solvent" to the longest chains.

These RDP equations produced a good fit to the extensional rheology of polydisperse polystyrene melts in [21], although overpredicted the modulus of the linear viscoelastic envelope. This may cause problems at low speeds in flow simulation, although the good predictions in the extension are promising for our simulations of geometries involving strong extensional flows.

In Secs. II and III, we show that excellent agreement between experiments and simulations for prediction of extrudate swell can be made for polydisperse polymers at a range of flow rates, when both friction reduction and polydisperse effects on extensional relaxation times are taken into account in the underlying rheological model. In Sec. II, we describe the experimental methods used for polymer characterization and analysis. In Sec. III, we describe the computational methodology by which these polymers were simulated. In Sec. IV A, we show MPR extrusion data for capillaries of different *l:d* ratios, in Sec. IV B, we describe the effect of friction reduction on results and in Sec. IV C, we describe the effect of polydispersity on extrudate swell and evaluate the success of the RDP equation. The modified versions of the Rolie-Poly model incorporating polydispersity and friction reduction are described in the Appendix.

TABLE I. Average molecular weight distribution data for all polymers used.

Polymer	M_w (kDa)	M_n (kDa)	Dispersity
PS350	350	116	3.01
P627-S	252	198	1.27
PS281	281	250	1.13

II. EXPERIMENTAL

A. Characterization (GPC/rheology)

The materials used in this study were linear polystyrenes (see Table I). The polymer PS281 was synthesized via anionic polymerization according to the procedure described in [26]. The polymer P627-S, obtained from PolymerSource, was synthesized using living anionic polymerization in tetrahydrofuran (THF) at −78 °C. PS350 was obtained from Sigma-Aldrich.

A gel permeation chromatography (GPC) characterization was performed on all polymers. The samples were all run using THF as the solvent at 35 °C. The instrument was a Viscotek TDA 302 instrument with a triple detector system.

Linear rheology was performed using a TA instruments Discovery HR2 rheometer. Frequency sweeps were performed at temperatures from 140 °C to 200 °C and at angular oscillation frequencies ranging from 0.1 rad s^{-1} to 600 rad s^{-1}. A 1% strain was used throughout so as to be within the linear response region of all the polymers. The geometry used was a 25 mm parallel plate geometry with a sample thickness of 1 mm.

The rheology of all polymers was time-temperature superposition shifted to 180 °C using the *RepTate* software[1] to obtain a master curve. The data were fitted using the linear theory of Likhtman–McLeish to obtain the entanglement time and the plateau modulus, Rouse time, and reptation time for each material. These are shown in Table II.

The monodisperse rheology was then fitted using a spectrum of Maxwell modes to give a spectrum of higher relaxation times and moduli, beyond the fundamental (reptation) mode. The lowest frequency mode is assigned the same

[1]The original *RepTate* software can be found at http://www.Reptate.com. An updated version is in development and can be found at https://reptate.readthedocs.io/.

TABLE II. Relaxation times for the single stretching mode of the polydisperse polymers at 180 °C. The molecular weight of P627-S shown is that of the highest M_w peak, rather than the average value shown in Table I.

Polymer label	Molecular weight (kDa)	Plateau modulus G_N^0 (MPa)	τ_R (s)	τ_d (s)
PS350	350	2.4788	0.17257	4.8993
P627-S	340	2.5600	0.16285	4.8357

relaxation time as the reptation time from the Likhtman–McLeish theory and the other modes are obtained via a best fit to the data.

Nonlinear extensional rheology in start-up flow was performed on each material using the sentmanat extensional rheometer (SER) attachment to the HR2 rheometer. The temperature of the environmental test chamber was maintained at 180 °C so as to ensure that the extensional data matched the linear shear data. The samples are melt pressed into a strip 20 mm by 10 mm by 1 mm thick and placed between the SER clips. The samples are equilibrated, pre-stretched for 10 s at a Hencky rate of 0.001 s^{-1} and then stretched at the required rate up to a Hencky strain of 3.8.

B. MPR measurements

The extrudate swell measurements were obtained within an MPR at 180 °C. The upper barrel and the upper half of the test section are filled with polymer, and the apparatus is heated to temperature. The polymer is left to melt and equilibrate for at least half an hour before the apparatus is sealed so as to compress the sample. The upper piston is lowered at a controlled velocity and thus the polymer is extruded through the capillary test section and into the free space within the bottom chamber, also held isothermally at 180 °C. The extrudate can be viewed for approximately 5 mm below the die exit through the quartz viewing windows. A schematic diagram of the apparatus is shown in Fig. 2.

The apparent shear rate at the capillary wall is calculated using Eq. (13) for a Newtonian melt. Real wall shear rates will of course differ and are captured in the simulations

$$\dot{\gamma}_w = \frac{4r_p^2 v_p}{r_{\text{cap}}^3}, \tag{13}$$

where r_p is the piston radius (5 mm), v_p is the downward velocity of the top piston, and r_{cap} is the radius of the MPR capillary. For all the results reported in Secs. IV B and IV C, $r_{\text{cap}} = 1$ mm, giving the 5:2 capillary die. In Sec. IV A, a 0.5 mm radius capillary is used to give a 5:1 capillary die. The swelling ratios are calculated by analyzing a snapshot of the flow at steady state using a commercial image analysis program.

III. THEORETICAL

A. Flowsolve

Flow velocities and stresses for the extrudate geometry were calculated using the *flowSolve* finite-element package. *flowSolve* is an adaptive Lagrangian scheme that has been used extensively for comparison with MPR experiments [19,27,28] and is detailed more comprehensively in our previous work [2] and elsewhere [29]. In summary, the simulation geometry is filled with a series of mesh points connected by triangular finite elements as shown in Fig. 3. Each point carries a velocity, and each triangle has a constant velocity gradient between each set of points. The triangles also carry an associated stress tensor, as well as constitutive model dependent parameters such as Rolie-Poly orientation, chain stretch, and (for the first time in these simulations) monomeric friction reduction coefficient. The geometry has an axis of rotational symmetry down the center, which allows a 2-dimensional simulation of the cylindrical die used in the MPR, so markedly reducing the time that would be required for simulation of the full geometry, at the cost of assuming axisymmetric flow at all times. As a balance between simulation speed and accuracy, the mesh is chosen to have a maximum triangle side length corresponding to 0.3 mm within the upper chamber. The maximum triangle length is reduced by a factor of ½ in the region around the die entry and exit corners. This method provides a good balance between short computation time (with a coarse mesh) and accuracy (very fine mesh). In our previous work, we showed that using a finer mesh than this has little effect on the extrudate swell results in the flow regimes of this study [2].

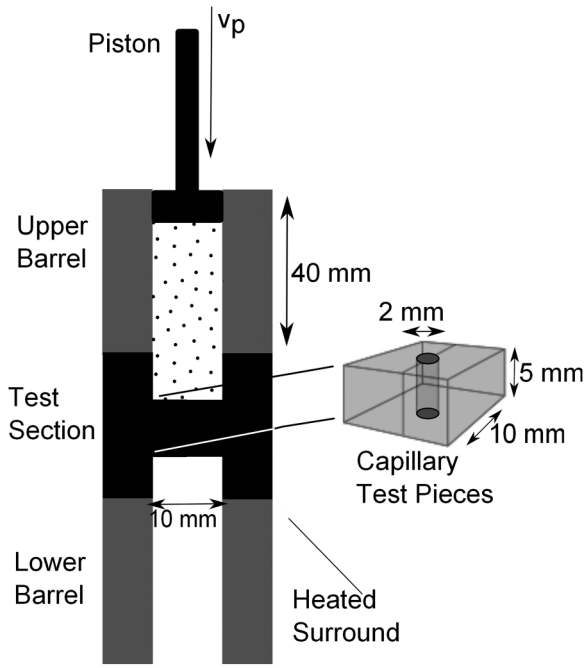

FIG. 2. The MPR 5:2 capillary geometry.

The velocities are solved at each point and at each simulation time step using standard equations for mass and momentum conservation

$$\begin{aligned} \nabla_i v_i &= 0, \\ \nabla_j \sigma_{ij} &= \nabla_i p - \mu \nabla^2 v_i. \end{aligned} \tag{14}$$

Once this step has been performed, the points are moved according to their velocity and then the constitutive equation is solved for each triangle. The stress calculated is then

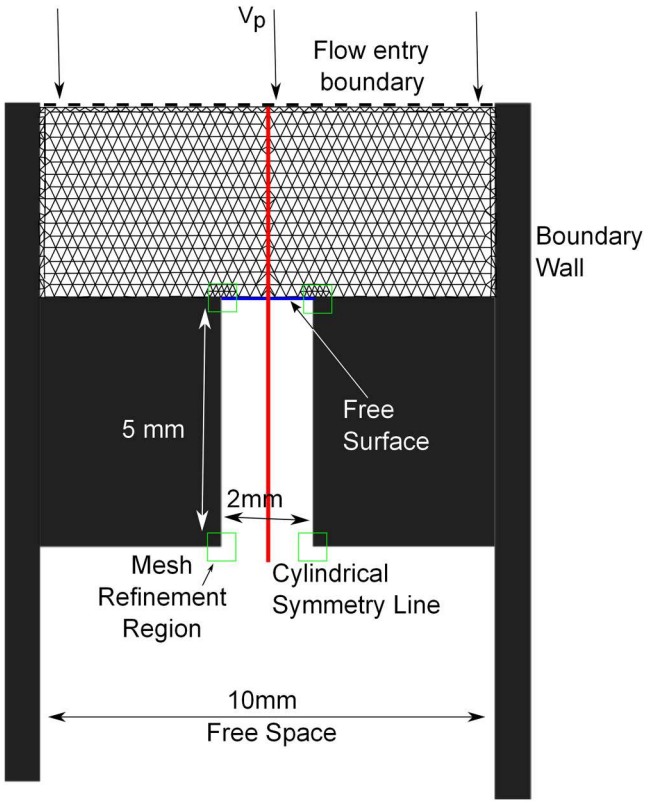

FIG. 3. The extrusion geometry used within the *flowSolve* simulations for a 5:2 capillary die.

used to solve the points again for their new velocities under the creeping flow requirement of zero force density. To ensure that the flow history prior to extrusion is properly modeled, the free-surface is initially positioned at the die entry and the flow is allowed to evolve within the die prior to extrusion. In practice, as the flow is taken at steady state, there is a little difference between simulations using this initial condition and those which the free-surface is initially positioned at the die exit.

The spatial region that has emerged to be of greatest interest for this work is the region around the die exit, where the no-slip boundary wall in the die meets the free-surface of the extrudate. The singularity in the velocity gradient induces a formal singularity in the stress, so needs careful handling computationally. In this work, the singularity was managed numerically by creating a special simulation point at the die exit corner. The point is allowed to have a nonzero velocity, and thus velocity gradients are calculated as if the point were moving. The point is, however, never moved from the corner so that, in this regard, the velocity is ignored. This method effectively negotiated the flow computation between the free flow and the fixed boundary without leading to divergences or instabilities. However, it maintained the calculation of the strong extensional stress generated by the formal singularity, whose physics is highly significant for the subsequent downstream shape of the extrudate flow.

A spectrum of Rolie-Poly elements is used in all simulations. If the reptation time of an element is less than 100 times the simulation time scale ($\dot{\gamma}^{-1}$), it is defined as being solvent and is used to create a background viscosity.

B. Monodisperse polymer modeling

Monodisperse simulations were performed using the finitely extensible Rolie-Poly equation described in Eq. (2). A finite extensibility of 5 was used for the single stretching element to be consistent with our previous monodisperse work, as well as earlier work on finite extensibility in [30] and references therein. The remaining Rolie-Poly elements were simulated using the nonstretch Rolie-Poly equation [Eq. (3)], and the properties are summarized in Table S1 of the supplementary material [32]. The detailed distribution of fast, nonstretching elements is not crucial for the results of the extrudate swell simulations. Their chief instrumental role is in defining the background viscous stress term that stabilizes the numerical method.

Two geometries were simulated: the 2 mm diameter die as given in Fig. 3 and a similar geometry with a die diameter of 1 mm.

Where friction reduction is required (Sec. IV B), the method outlined in Sec. IV C is used to calculate variable relaxation times for each individual simulation triangle.

C. Polydisperse polymer modeling

1. Single stretching mode Rolie-Poly approximation

A first, rough, approximation to the polydisperse and bidisperse polymers, useful as a benchmark for evaluation of the more detailed polydisperse models, assumes a single Rouse relaxation time as for the monodisperse polymers. The polydisperse polymers are allocated the same entanglement molecular weight as in the monodisperse case, i.e., 16.5 kDa. The M_w of the polymers is normalized by M_e to give a value for Z, and thus a value for the Rouse relaxation time can be calculated using Eq. (1) and the fitted value of τ_e. The values obtained using this method for the polymers PS350 and P627-S are shown in Table II.

The remaining nonstretching Rolie-Poly elements within the simulations are taken to have the same moduli and relaxation times as the remaining Maxwell modes from the linear rheological fit.

2. Polydisperse theory

To treat the polydisperse materials as faithfully as possible, we use, as introduced above, the RDP model developed by Boudara *et al.* [21,22] and described in the Appendix.

The simulations work with a model of each melt containing 9–12 Rolie-Poly elements. In the monodisperse simulations, these corresponded to a series of Maxwell modes from the linear rheology, each with a modulus and relaxation time as well as Rouse times and $\lambda_{\max}$ values attached. However, in the polydisperse case the Rolie-Poly elements are derived from individual molecular weights from a discretized molecular weight distribution.

The entanglement times and moduli for the samples are extracted from the linear rheology. The molecular weights and fractions for each element are calculated by discretizing the molecular weight distribution into 9–12 bins using *RepTate* to obtain a series of masses and fractions.

These masses are normalized by the entanglement molecular weight of 16.5 kDa to give a series of effective Z values for each element. To obtain a series of Rouse and reptation times for each element, Eq. (1) is used to obtain an initial guess. However, this initial guess fails to take into account that the tube formed by the chains of a particular molecular weight is diluted by the other molecular weight chains in the blend. The Z values must then be replaced by an effective diluted number of entanglements, Z_{eff}

$$\begin{aligned} Z_{\text{eff}} &= Z\phi_{\text{dil}}, \\ \tau_{d,\text{eff}} &= 3\tau_e Z^3\left(1-\frac{3.38}{\sqrt{Z_{\text{eff}}}}+\frac{4.17}{Z_{\text{eff}}}-\frac{1.55}{Z_{\text{eff}}^{3/2}}\right), \\ \tau_{R,\text{eff}} &= \frac{\tau_R}{\phi_{\text{dil}}}. \end{aligned} \tag{15}$$

The dilution parameter ϕ_{dil} is worked out iteratively for each element using the following equation:

$$\phi_{\text{dil},i} = \sum_{j_{\min}}^{N_{\text{modes}}} \phi_j, \tag{16}$$

where $j_{\min}$ is the highest index element such that $\tau_{R,\text{eff},i} > \tau_{d,\text{eff},j}$ and ϕ_j is the weight fraction of chains represented by element j. Thus, a molecular weight i is diluted by a lower molecular weight j if the terminal relaxation time of the fraction j is shorter than the effective Rouse time of i. The convective constraint release coefficient, β, is assumed to be 0.5 as in [2] and [31]. Consistent with our previous work and the simulations of Boudara, we take $\lambda_{\max}$ to be 5 for all modes.

Three polymers were simulated using this theory: the near-monodisperse sample PS281, the bidisperse polymer P627-S, and the polydisperse polymer PS350. The molecular weight distributions are shown in Fig. 4, and the spectrum of Rolie-Poly elements produced for P627-S is shown in Table III. The other spectra can be found in the supplementary material [32].

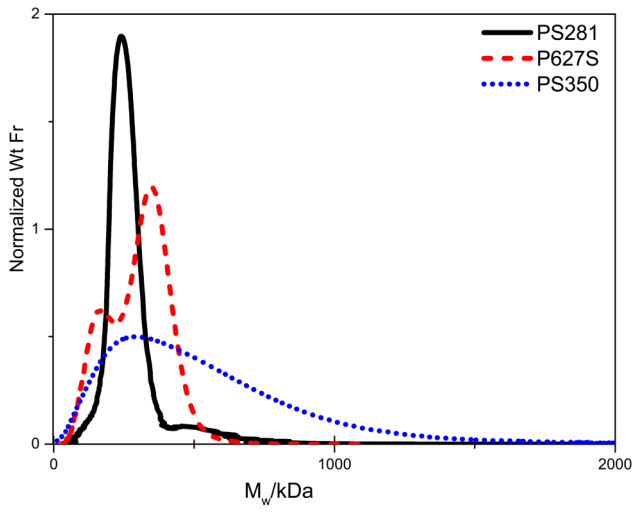

FIG. 4. Molecular weight distributions for the monodisperse, bidisperse, and polydisperse polymers reported here.

TABLE III. Summary of Rolie-Poly elements for P627-S. Reptation and Rouse relaxation times are given at 180 °C. The plateau modulus G_N^0 is 2.4788×10^5 Pa, and the entanglement time is 0.00038 s.

Element index	Molecular weight (kDa)	Weight fraction	τ_d (s)	τ_R (s)
1	75	0.0194756	0.0093476	0.00795496
2	107	0.062089	0.0348345	0.0161507
3	147	0.126734	0.112358	0.0304008
4	183	0.0806178	0.250364	0.0472143
5	208	0.054925	0.397923	0.0611144
6	234	0.0684394	0.600079	0.0769976
7	267	0.0676063	0.958645	0.100466
8	323	0.145531	1.8693	0.147637
9	401	0.215954	3.89571	0.226979
10	479	0.120631	7.10907	0.324487
11	563	0.0318184	12.1402	0.447937
12	675	0.00617869	21.9834	0.643365

If we treat the blend P627-S as a purely bidisperse melt of 340 and 160 kDa chains as in [2], we would not expect the stretch time enhancement of 340 kDa chains by dilution with 160 kDa chains as, according to the modified Viovy diagram [23], they are not significantly separated in molecular weight. However, as this sample is not purely bidisperse, but rather consists of two broadly polydisperse peaks, we would expect stretch time enhancement of the highest molecular weight chains and some of the intermediate chains by the very shortest chains. This will lead to a slight enhancement in the average stretch relaxation time of the whole melt.

IV. RESULTS AND DISCUSSION

In this section, we describe three sets of results. In Secs. IV A and IV B, we use monodisperse polymers to determine the relative importance of geometrical and constitutive parameters before extending to polydisperse samples in Sec. IV C. For monodisperse polymers, Sec. IV A describes the limited effect changing of *l:d* ratio on swelling ratios, and Sec. IV B shows the effect of reducing monomeric friction on results at high shear rates.

A. The effect of die geometry on swelling ratio

The results obtained using the 5:1 ratio capillary die are shown in Fig. 5 alongside the results for the 5:2 capillary die used in the previous work.

As in our previous publication [2], the *flowSolve* predictions for the 5:1 capillary agree with the MPR data up to a $W_R \sim 7$, after which point the data plateau slightly before continuing to increase at a swelling ratio, now consistently below the predictions. The simulations in Fig. 5 do not predict any significant difference between the B values for the $l{:}d = 5{:}1$ and 5:2 capillaries until $W_R = 13$. It is not possible within the current geometry to show whether this trend is matched within the MPR experiments; it is only possible to say that no difference (outside error) between the two geometries is seen and that this is consistent with the modeling.

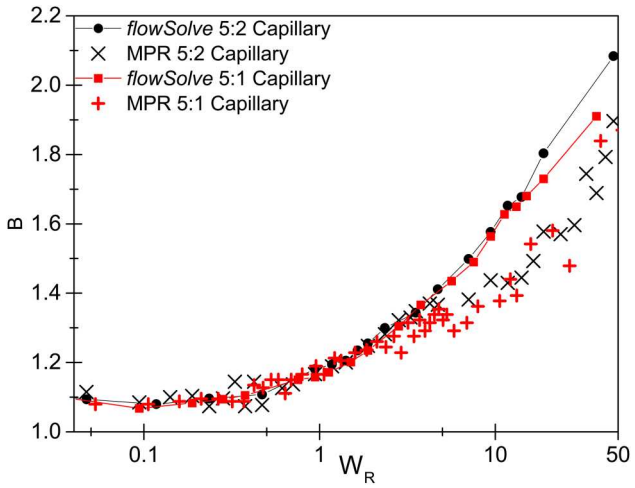

FIG. 5. Comparison of MPR data (points) and *flowSolve* predictions using the single stretching mode Rolie-Poly equation (lines) for PS281 within 5:2 and 5:1 *l:d* ratio capillaries.

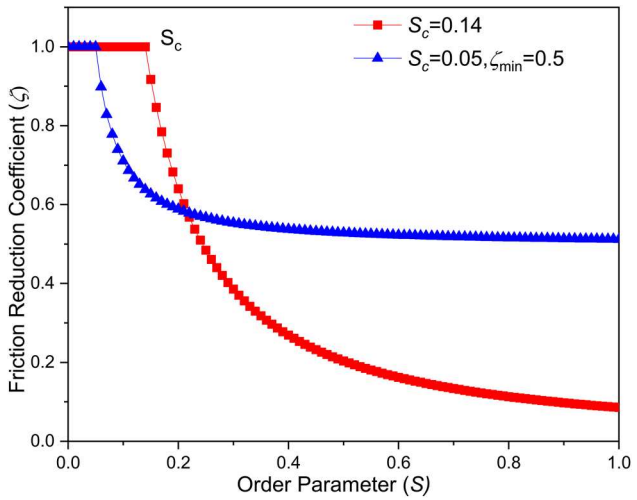

FIG. 6. The effect of changing the value of S (the order parameter) upon the friction reduction coefficient ζ and thus the relaxation times.

The disagreement between theory and experiment occurs at the same Weissenberg number, despite the different capillary geometry. Crucially within the MPR, these correspond to different piston velocities, v_p. $W_R = 7$ occurs at $v_p = 0.13\ \text{mm s}^{-1}$ for the 5:1 geometry and at $1.5\ \text{mm s}^{-1}$ for the wider capillary. The experimentally measured pressure drops along the MPR capillary are also different, 33 ± 2 bar for the 5:1 capillary and 20 ± 1 bar for the 5:2 capillary. The fact that these parameters are different and yet the disagreement with theory still occurs at the same W_R indicates that the disagreement is due to a material property and not due to systematic experimental errors.

B. Friction reduction

The model used for friction reduction in this work is described by Eq. (7), which has an added minimum friction term, modifying the model used by others described by Eq. (5). Three parameter sets are used to determine the magnitude of the friction reduction: the parameters of Yaoita *et al.* ($S_c = 0.14$) and two best fit parameter sets, ($S_c = 0.05$, $\zeta_{\text{min}} = 0.5$ and $S_c = 0.0235$, $\zeta_{\text{min}} = 0.819$). The effect of an increase in order parameter on ζ, which in turn reduces τ_d and τ_R for these two parameter sets is shown in Fig. 6.

Introducing a minimum friction term means that the friction changes very little at high order parameters, but there is still a large drop in friction at low order parameters above the critical value. This should give a large effect at medium flow speeds ($W_R > 1$) but a decreasing effect at high flow speeds ($W_R \gg 1$).

A test of the friction reduction equations, independent of the complex deployment within the extrudate swell simulations, is their more straightforward effect on uniaxial extensional rheology. Predictions with and without friction reduction are shown in Fig. 7.

Using a value of $S_c = 0.14$ has no effect on the uniaxial extensional predictions below rates of $50\ \text{s}^{-1}$ and little effect at or above this rate, so is omitted from the diagram. Only the highest extension rates result in order parameters above the critical value and thus result in a decrease in friction. Using a lower S_c gives a much larger effect, a decrease in the steady-state plateau and a slight decrease in the transient viscosity prediction leading up to the plateau.

Using friction reduction improves the fit to the SER data at $40\ \text{s}^{-1}$, giving an approximately correct high strain plateau. At higher shear rates, however, the friction reduction with $\lambda_{\text{max}} = 5$ results in a steady-state plateau at too low a viscosity. Using a higher λ_{max} of 6 is necessary here to give an improved steady-state plateau, closer to the high viscosity limit of the experimental data. It is not possible with the SER setup to measure the steady-state extensional viscosity, but it seems that simulations including friction reduction would underpredict this viscosity.

Figure 8 shows the predictions of the modified model with a minimum friction constant [Eq. (7)] with differing friction reduction parameters.

Also shown are the best fit parameters for Eq. (7), obtained from fitting to the extensional data ($\lambda_{\text{max}} = 6$, $\zeta_{\text{min}} = 0.5$ $S_c = 0.05$) and the extrudate swell data ($\lambda_{\text{max}} = 5$, $\zeta_{\text{min}} = 0.5$, $S_c = 0.05$). The two parameters of the friction reduction model, S_c and ζ_{min}, have different effects; S_c governs the Weissenberg number at which the results deviate from the standard predictions. $S_c = 0.14$ gives a deviation at $W_R = 9$. The ζ_{min} term, on the other hand, governs the B value reached at high shear rates. Not including a ζ_{min} term results in a plateau in extrudate swell above these critical Weissenberg numbers. This is because the chain stretch values approach λ_{max} and thus the chain order parameter rapidly approaches 1. This means that almost no additional stretch can be built up at chain orientations above S_c. The inclusion of a ζ_{min} means that the chain stretch can increase after the orientation is above S_c. This allows the extrudate swell ratios to continue to increase albeit shifted to higher rates due to the lower stretch built up within the extruder.

The parameters $\zeta_{\text{min}} = 0.5$ and $S_c = 0.05$ fit the extrudate swell well but, as shown in Fig. 7, underestimate the steady-state viscosity under uniaxial extension with the λ_{max} value of 5 used previously. Using a slightly increased λ_{max} value of 6 results in an improved fit to the uniaxial extension but,

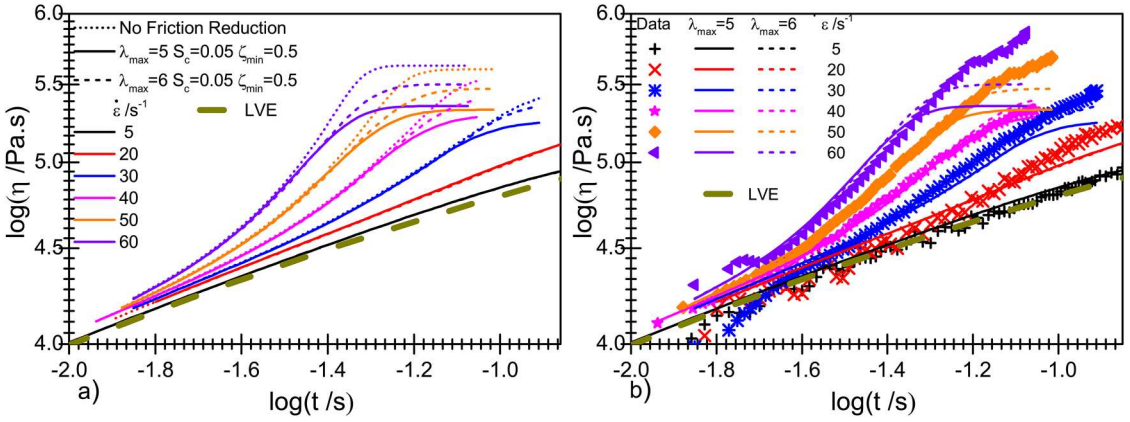

FIG. 7. The effect of friction reduction on predictions of uniaxial extension using the Rolie-Poly model for PS281. (a) shows predictions using different finite extensibility parameters and (b) shows the comparison of the Rolie-Poly model and the two sets of parameters to SER data. The Rolie-Poly linear viscoelastic envelope (LVE) is also shown. All theory predictions converge on this envelope at shorter times than shown in this figure.

although capturing the extrudate swell at W_R up to 7, and beyond 30, does not give a large enough decrease in B values at intermediate values of W_R of order 10. The current theory cannot simultaneously produce accurate predictions for both sets of experimental data throughout the full extent of their range. For the remainder of this work, we continue with the parameters $\lambda_{\max} = 5$, $\zeta_{\min} = 0.5$, and $S_c = 0.05$, which work well for extrudate swell, and note that the model cannot give accurate predictions of both uniaxial extension and the complex system of extrudate swell. Future work on this topic may include the use of an alternative measurement system such as a filament stretching rheometer, which can obtain the higher strains required to thoroughly test the model.

As with chain stretch, the friction reduction coefficient from the simulations can be plotted as a function of radius and distance along the capillary die (Fig. 9).

The friction reduction coefficient shows a similar trend to chain stretch as a function of distance along the capillary. At the die entry, ζ is low, meaning short relaxation times. Chain stretch can thus relax quickly. There is a trough in ζ at the die exit corresponding to the chain stretch peak observed at the same point. The friction reduction switches on a lot more sharply than the stretch, due to its critical onset and rapid saturation at high Weissenberg numbers where the wall stretch approaches $\lambda_{\max}$.

We can now calculate the effect of reduction of friction on the chain stretch along the die, shown in Fig. 10.

For Weissenberg numbers slightly above 1, there is almost no effect of reducing the monomeric friction (the lower lines in Fig. 10). The steady-state chain stretch along the capillary wall is reduced, although this has little effect upon the peak in the stretch at the die exit corner. At much higher Weissenberg numbers, chain stretch values are significantly reduced both at the capillary wall and at the die exit corner. The magnitude of friction reduction increases with increasing chain stretch. The reduction in chain stretch shown in Fig. 10 is the reason that the extrudate swell values are reduced at

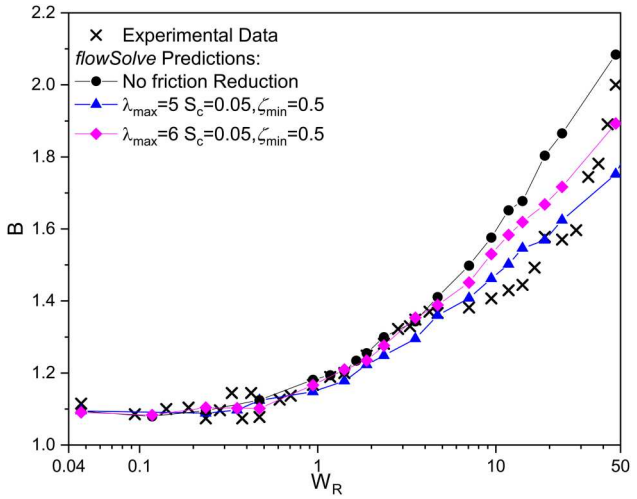

FIG. 8. The effect of including monomeric friction reduction on extrudate swell simulations using the single stretching mode Rolie-Poly model and comparison to the experimental data for PS281.

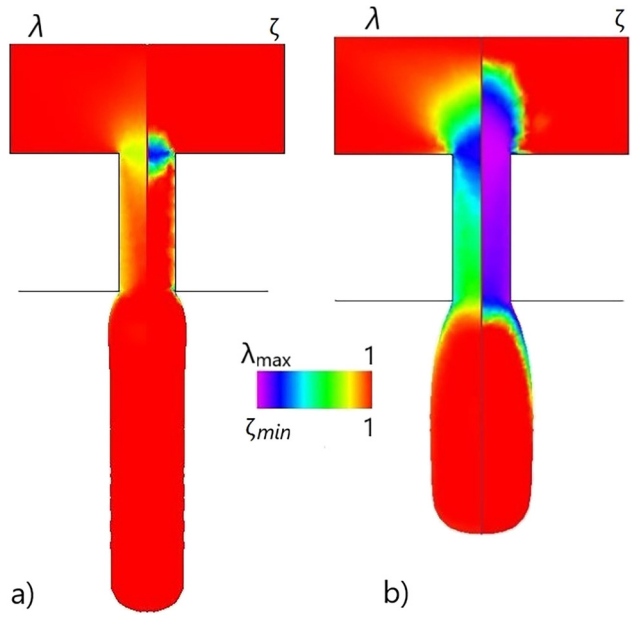

FIG. 9. The values of chain stretch, λ, (left) and friction reduction coefficient, ζ, (right) along the capillary at (a) $W_R = 4.7$ and (b) $W_R = 47$ for PS281 with $S_c = 0.05$ and $\zeta_{\min} = 0.5$.

these high Weissenberg numbers, as the extrudate swell is heavily dependent on chain stretch at the wall and the exit corner. If the alternative set of friction reduction parameters was used then the reduction in chain stretch at W_R would be less and the two chain stretch curves at each Weissenberg number in Fig. 10 would be closer together.

C. Polydisperse theory

To test the RDP model within the context of extrudate swell, we first simulate the monodisperse polymer PS281 as a benchmark. This will test to see if the method of calculating the time scales of the Rolie-Poly elements described earlier is consistent with the method of using Maxwell modes used previously. Predictions of nonlinear extension for both models are shown in Fig. 11.

The Rolie-Poly and RDP models produce very similar predictions for extensional viscosities. The long time, high strain predictions are almost identical for both models, and there are only minor differences otherwise. The largest difference is in the short-time prediction for $5\,s^{-1}$, where the viscosity is underpredicted by the RDP model. This should not be consequential for prediction of extrudate swell, as the predictions of the onset of strain hardening and steady-state viscosities are more relevant. These predictions for extrudate swell are shown in Fig. 12 both without friction reduction and with $\lambda_{max} = 5$, $S_c = 0.05$, and $\zeta_{min} = 0.5$.

The Rouse Weissenberg number is calculated using the same Rouse time as the monodisperse case, i.e., 0.047 s. The RDP model without friction reduction shown in Fig. 12 produces the same results as the monodisperse prediction up to $W_R = 5$, where the data start to deviate from experimental measurements. Above this point, the trend of the data is the same as the monodisperse simulation, but the simulation results are slightly less consistent and the increase in extrudate swell occurs less smoothly. Predictions of the RDP model including friction reduction also produce similar results to the friction reduced Rolie-Poly predictions, giving an improved agreement with experimental

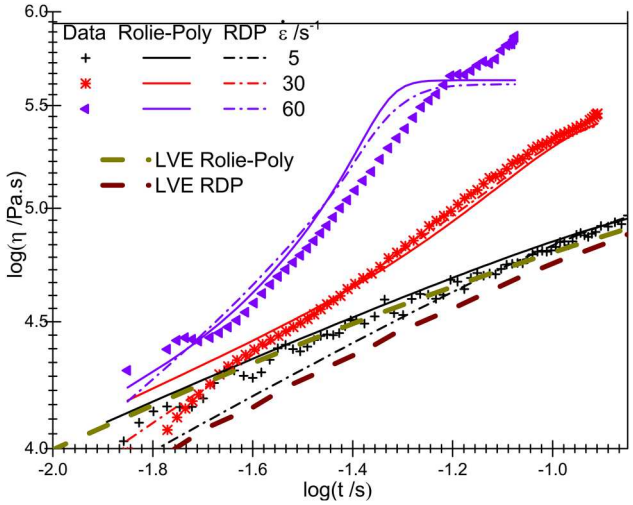

FIG. 11. Comparison of uniaxial extensional predictions for PS281 using the Rolie-Poly (——) and RDP (- -) models without friction reduction.

data at high Weissenberg number. This is due to the high chain stretch values in the highest molecular weight elements causing large deformations in the finite-element mesh at the highest speeds.

Predictions for the uniaxial extension of bidisperse sample P627-S are shown in Fig. S1 in the supplementary material [32]. The RDP model roughly predicts the onset of strain hardening and the extensional viscosities up to $10\,s^{-1}$. Above this rate, extensional viscosities are overpredicted similarly to the monodisperse sample.

Figure 13 shows the extrudate swell for P627-S. The W_R values are calculated using the Rouse times in Table II, the Rouse time for a chain of the same M_w as the peak M_w. The RDP model predicts the low Weissenberg number extrudate swell much better than the 1 mode prediction; but as the Weissenberg number is increased to ~1, both theories underpredict the swelling ratios by a similar amount.

In our previous work, we described a better fit by increasing the stretch relaxation time by hand, according to the

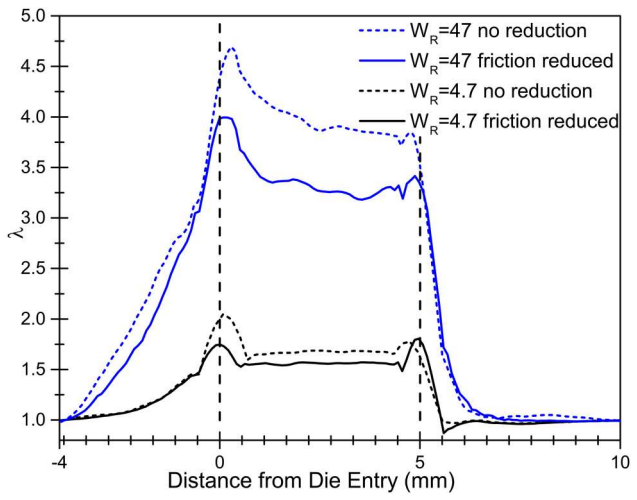

FIG. 10. Simulated chain stretch along the wall of the 5 mm capillary for PS281 at $W_R = 4.7$ and $W_R = 47$ for friction reduction with $S_c = 0.05$ and $\zeta_{min} = 0.5$ enabled and disabled.

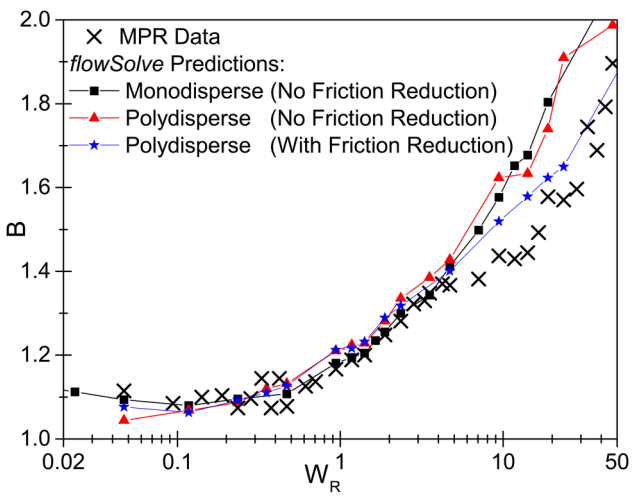

FIG. 12. Comparison of MPR data of PS281 at 180 °C to the polydisperse RDP predictions within *flowSolve* of PS281.

weight fraction of long chains in the blend. This resulted in the Rouse time of the 340 kDa chains in the blend being increased from 0.16285 to 0.2585 s. However, using RDP, this manual intervention is no longer required. Instead, an increased Rouse time for diluted high molecular weights occurs naturally as a result of the coupled constraint release term in Eq. (A4) of the RDP equation set. This effective increase in Rouse time only occurs for relatively low values of chain stretch and is not sufficient to give the increase in extrudate swell seen at intermediate shear rates (around $W_R = 1$). A slightly improved prediction at the lowest shear rates is obtained with the low shear rate swelling ratios matching those of the MPR, although this improvement does not extend above $W_R = 1$. To improve the prediction at these intermediate deformation rates, it may be necessary to change the parameterization of the slower (higher molecular weight) elements to increase the Rouse times used as inputs to the model rather than allow them to "effectively" increase during running of the simulation. Doing this points to physics not captured by the nonlinear polydisperse tube theory to date. This may also worsen the agreement of the RDP model to SER data at low strain rates.

Due to the discretization of the molecular weight distribution, it is now possible to calculate the chain stretch of each individual molecular weight fraction under different flow conditions. This is shown in Fig. 14.

The highest molecular weight chains are stretched significantly even at low W_R. Even below $W_R = 1$, these chains are still stretched to $\lambda > 3$ at the die exit corner. This significant chain stretch will contribute greatly to the increased swelling ratios compared to the monodisperse case. The simple monodisperse model used previously cannot account for the fact that high molecular weight fractions are significantly stretched at low Weissenberg numbers, instead of showing a single, low, average stretch across all chains.

We can now address the polydisperse sample PS350. Uniaxial extensional predictions using both the Rolie-Poly and RDP model are shown in Fig. 15.

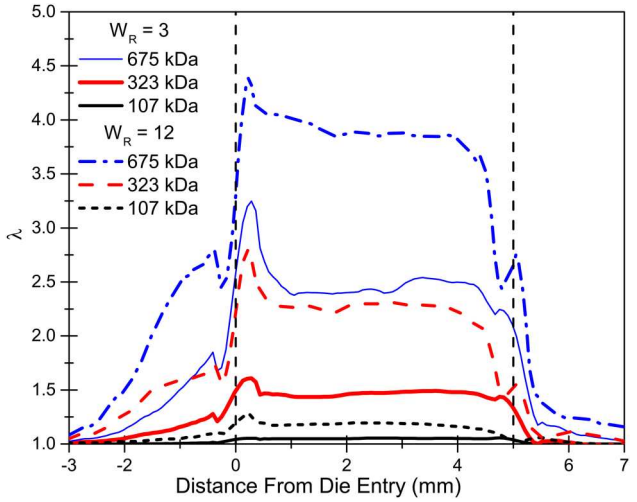

FIG. 14. Wall chain stretch values along an extrusion die for P627-S elements 2, 8, and 12 from Table II. Rouse Weissenberg numbers of 3 and 12 correspond to solid and dashed lines, respectively.

Using a single Rouse time in the Rolie-Poly model results in significantly underpredicted extensional viscosities for PS350 at low rates. PS350 begins to strain harden at approximately $1\,s^{-1}$ or more, but this is not predicted using Rolie-Poly until $\sim 10\,s^{-1}$. However, the RDP model accurately predicts the onset of strain hardening at these lower and intermediate rates, although increasingly overpredicts the extensional viscosities until the predictions at the highest strain rates become significantly worse than the standard Rolie-Poly prediction. At a W_R of 17, the simulated extension rate at the die exit corner for this sample is greater than the highest strain rate achievable in the SER. It would therefore be expected that the extension rate overprediction would slightly affect the extrudate swell predictions. Friction reduction using the parameters $\lambda_{max} = 5$, $S_c = 0.05$, and $\zeta_{min} = 0.5$ has little effect here; it slightly, but not significantly, reduces the overprediction in extensional viscosities at the highest rates. This reduction is

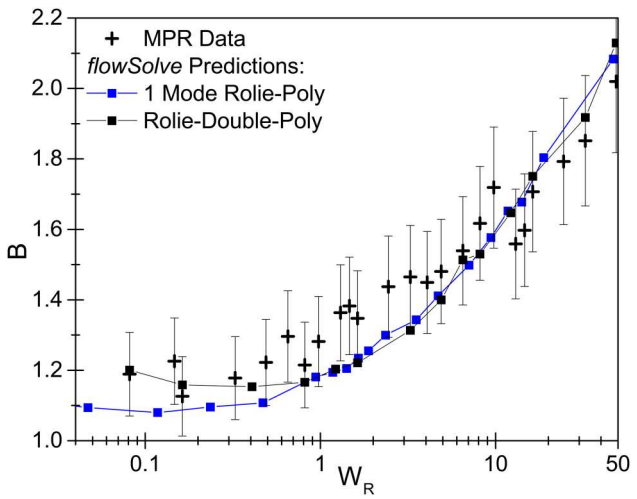

FIG. 13. Comparison of MPR data of P627-S at 180 °C to the RDP theory predictions within *flowSolve* of P627-S and a 1-mode prediction using standard Rolie-Poly within *flowSolve*.

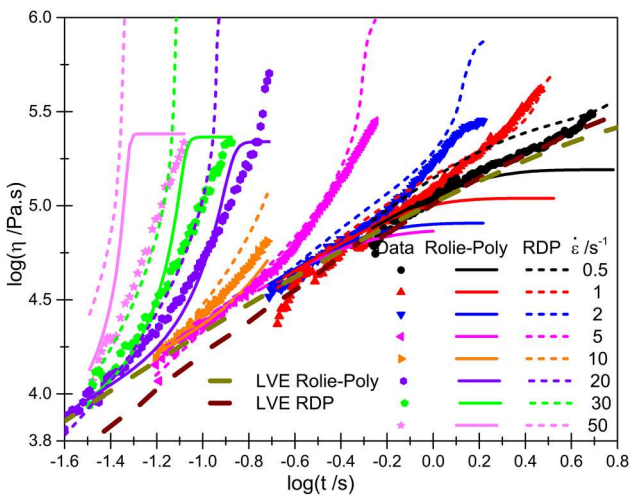

FIG. 15. Rolie-Poly (lines) and RDP (dashed lines) predictions for uniaxial extension for PS350 overlain on SER data. The linear viscoelastic envelope (LVE) for each model is shown as a dashed line.

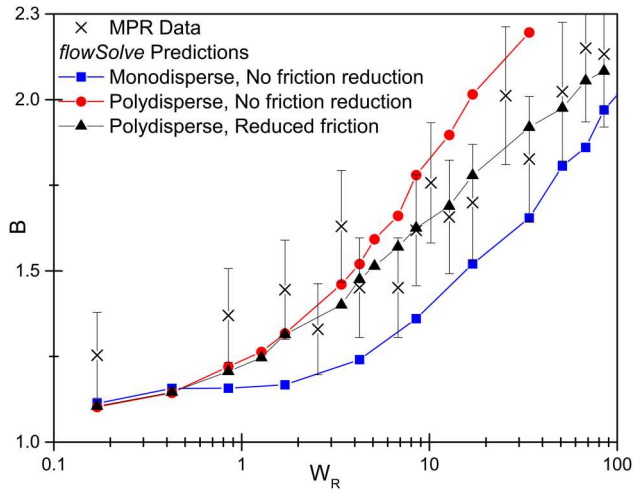

FIG. 16. Extrudate swell predictions for PS350 at 180 °C using monodisperse Rolie-Poly and the polydisperse RDP theory with/without friction reduction. The Rouse times are calculated using the average time scales in Table II.

much smaller than that shown in Fig. 7 for the monodisperse sample.

The polydisperse predictions for swelling ratios in PS350 are compared to the MPR swelling ratios in Fig. 16.

As with the bidisperse polymer, using a single Rouse time for the polydisperse polymer is not an acceptable way of modeling the extrudate swell. The polymer swells much more strongly at $W_R \sim 1$ than would be expected from a melt with a single dominant Rouse time. This is due to high molecular weight fractions in the blend stretching at their own effective Rouse times. The RDP theory gives a good prediction for the onset of extrudate swell. Some overprediction of swelling is seen above $W_R = 10$ here. However, as with the monodisperse simulations, using friction reduction at high shear rates results in a good fit to the experimental data. Crucially, the parameters $S_c = 0.05$ and $\zeta_{\min} = 0.5$ used here are the same as those that gave the best fit to extrudate swell for the monodisperse sample. The friction reduction has less of an effect on the polydisperse simulations than it does on the monodisperse ones. This difference is due to the presence of low molecular weight chains that are only slightly stretched at high shear rates. These chains have a low ζ and thus serve to limit the effect of friction reduction—the monomer environment is less perturbed from equilibrium by strong flows. Conversely, the presence of the high molecular weight chains means that the friction reduction reduces extrudate swell at lower Weissenberg number than in the monodisperse case. It is clear from these results that both a polydisperse theory and friction reduction are required to obtain good predictions for extrudate swell.

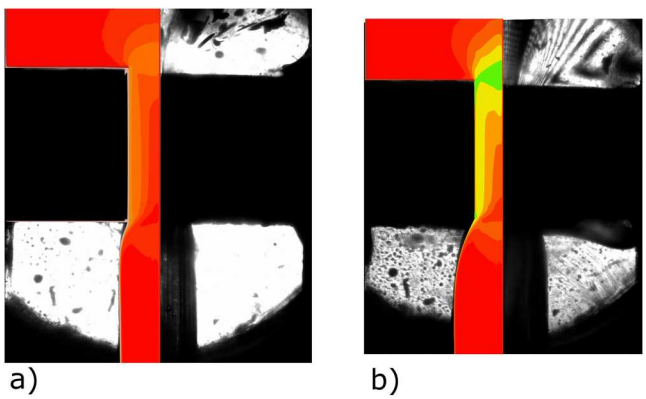

FIG. 17. Comparison of extrudate images obtained from simulation (left) and experiment (right) for PS350 at (a) $W_R = 1.7$ and (b) $W_R = 17$ with friction reduction. Shading shows simulated first normal stress difference.

Example extrudate profiles from the MPR and from *flowSolve* are shown in Fig. 17.

The simulated profile for $W_R = 1.7$ appears consistent with the experimental profile. It is difficult to compare the profile for $W_R = 17$ due to the limited viewing area within the MPR lower section. The maximum swelling ratio occurs further away from the die exit for the higher speed. However, within this limitation, the maximum swelling observed and predicted appears to be consistent with each other.

V. CONCLUSIONS

We have shown that the RDP model combined with a finite-element simulation package is capable of producing good predictions of extrudate swell up to high Weissenberg number for both near-monodisperse and polydisperse polystyrenes over most of a three-decade range of flow rates. Reducing the monomeric friction coefficient is essential when predicting behavior for Rouse Weissenberg numbers above ~7, where the monomer orientation (in polystyrene polymers) is strongly perturbed from equilibrium and where the swelling ratio would be significantly overpredicted otherwise. Viscometric and extrudate swell data together constitute very strong constraints on the model, indicating that there remain some unexplained features at intermediate rates, including the strength of a plateau in swell as friction reduction first sets in.

Using a recently developed multimode blended version of the Rolie-Poly model (RDP), containing an approximation of tube relaxation acceleration through constraint release, results in good qualitative predictions for polydisperse polymers, although the model performs less well for the low shear rate extrudate swell of a bimodal blend. The multiscale modeling approach we present here allows us to identify the cause as an insufficient increase in the longest stretch relaxation time upon dilution. The length to diameter ratio of the extrusion die can be included explicitly but is not a significant factor affecting the swelling ratios at the shear rates used in these studies, on which the experiments and calculations agree.

Future work will involve extension of the polydisperse simulations to systems with a higher polydispersity and/or a more complex molecular weight distribution. Within this methodology of molecular modeling of carefully controlled materials, yet in sufficient quantity to measure in complex flow such as extrusion, we will use polymers with controlled levels of branching to determine how branching effects swelling at well-defined flow speeds.

ACKNOWLEDGMENTS

The authors thank Dr. Dave Hoyle for help with the *flowSolve* software as well as Dr. Tim Nicholson for assisting with incorporating the new theories within *flowSolve*.

The authors also thank Carl Reynolds and Dr. Stephen Boothroyd for experimental help and Jon Millican for characterizing the polymers. This work was supported by the Engineering and Physical Sciences Research Council CDT in Soft Matter and Functional Interfaces (SOFI) Grant Ref. No. EP/L015536/1.

APPENDIX: RHEOLOGY THEORY

Here, we describe the polydisperse RDP equation set of Boudara *et al.* [21,22] and our modifications to it.

We can consider the overall stress of the blend as a weighted sum of the individual stresses on each individual molecular weight fraction

$$\boldsymbol{\sigma} = G_N^0 \sum_{i=1}^{n} (\phi_i F(\lambda_i) \mathbf{A}_i), \tag{A1}$$

where G_N^0 is the plateau modulus of the material, ϕ_i, $F(\lambda)$ is the finite extensibility function, and $\mathbf{A}_\mathrm{i}$ is the average conformation tensor of an entanglement segment of chain i. Boudara *et al.* calculate $F(\lambda)$ and λ using formulas

$$\begin{aligned} F(\lambda) &= \frac{1-\lambda_{\max}^{-2}}{1-\lambda^2\lambda_{\max}^{-2}}, \\ \lambda &= \sqrt{\frac{\mathrm{trace}(\mathbf{A})}{3}}, \end{aligned} \tag{A2}$$

which are valid for all components of the blend. Here, λ is the chain stretch and $\lambda_{\max}$ is the finite extensibility of the chains. Individual chain conformation tensors are calculated using

$$\mathrm{A}_i = \sum_{j=1}^{n} \phi_j \mathbf{A}_{i,j}, \tag{A3}$$

$$\begin{aligned} \frac{d\mathbf{A}_{ij}}{dt} =& \boldsymbol{\kappa}\mathbf{A}_{ij} + \mathbf{A}_{ij}\boldsymbol{\kappa}^T - \frac{1}{\tau_{d,i}}(\mathbf{A}_{ij} - \mathbf{I}) - \frac{2}{\tau_{R,i}}\left(\frac{\lambda_i - 1}{\lambda_i}\right) F(\lambda_i)\mathbf{A}_{ij} \\ & - \frac{1}{\tau_{d,j}}(\mathbf{A}_{ij} - \mathbf{I}) - \frac{2\beta}{\lambda_i\tau_{R,j}}\left(\frac{\lambda_j - 1}{\lambda_j}\right) F(\lambda_j)(\mathbf{A}_{ij} - \mathbf{I}). \end{aligned} \tag{A4}$$

This equation contains a mixed constraint release term. This term utilizes the chain stretch in both i and j chains but only the stretch relaxation time of j chains. This coupling term gives rise to the enhanced stretch relaxation time of the long chains predicted earlier. However, this enhancement in stretch time only occurs at small values of λ, i.e., $1 < \lambda < 2$, otherwise the stretch time is not enhanced.

The only difference in our simulations versus the equation set above is the exact form used for the finite extensibility. For consistency within *flowSolve*, we use the *Pade* approximant to the Inverse Langevin function $F(\lambda)$ used in the following equation:

$$F(\lambda) = \left(\frac{\lambda_{\max}^2 - \lambda^2/3}{\lambda_{\max}^2 - \lambda^2}\right)\left(\frac{\lambda_{\max}^2 - 1}{\lambda_{\max}^2 - 1/3}\right). \tag{A5}$$

The friction reduction method described in Sec. I C is used in several simulations. The method used is identical although the average orientation tensor from Eq. (8) is worked out using

$$\bar{\mathbf{S}} = \sum_{i=1}^{N_{\mathrm{modes}}} \phi_i \times \mathbf{A}_i / \mathrm{trace}(\mathbf{A}_i), \tag{A6}$$

instead of the assuming equal weighting as in Eq. (8).

REFERENCES

[1] Konaganti, V. K., M. Derakhshandeh, M. Ebrahimi, E. Mitsoulis, and S. G. Hatzikiriakos, "Non-isothermal extrudate swell," Phys. Fluids **28**, 123101 (2016).

[2] Robertson, B., R. L. Thompson, T. C. B. McLeish, and I. Robinson, "Theoretical prediction and experimental measurement of isothermal extrudate swell of monodisperse and bidisperse polystyrenes," J. Rheol. **61**, 931–945 (2017).

[3] Tanner, R. I., "A theory of die-swell," J. Polym. Sci. B Polym. Phys **8**, 2067–2078 (1970).

[4] Tanner, R. I., "A theory of die-swell revisited," J. Nonnewton. Fluid **129**, 85–87 (2005).

[5] Liang, J.-Z., "Estimation of die-swell ratio for polymer melts from exit pressure drop data," Polym. Test. **20**, 29–31 (2000).

[6] Liang, J.-Z., "A relationship between extrudate swell ratio and entry stored elastic strain energy during die flow of tyre compounds," Polym. Test. **23**, 441–446 (2004).

[7] den Doelder, C. F. J., and R. J. Koopmans, "The effect of molar mass distribution on extrudate swell of linear polymers," J. Nonnewton. Fluid **152**, 195–202 (2008).

[8] Likhtman, A. E., and R. S. Graham, "Simple constitutive equation for linear polymer melts derived from molecular theory: Rolie–Poly equation," J. Nonnewton. Fluid **114**, 1–12 (2003).

[9] Likhtman, A. E., and T. C. B. McLeish, "Quantitative theory for linear dynamics of linear entangled polymers," Macromolecules **35**, 6332–6343 (2002).

[10] Graham, R. S., A. E. Likhtman, T. C. B. McLeish, and S. T. Milner, "Microscopic theory of linear, entangled polymer chains under rapid deformation including chain stretch and convective constraint release," J. Rheol. **47**, 1171–1200 (2003).

[11] Ianniruberto, G., A. Brasiello, and G. Marrucci, "Simulations of fast shear flows of PS oligomers confirm monomeric friction reduction in fast elongational flows of monodisperse PS melts as indicated by rheooptical data," Macromolecules **45**, 8058–8066 (2012).

[12] Yaoita, T., T. Isaki, Y. Masubuchi, H. Watanabe, G. Ianniruberto, and G. Marrucci, "Primitive chain network simulation of elongational flows of entangled linear chains: Stretch/orientation-induced reduction of monomeric friction," Macromolecules **45**, 2773–2782 (2012).

[13] Auhl, D., P. Chambon, T. C. B. McLeish, and D. J. Read, "Elongational flow of blends of long and short polymers: Effective stretch relaxation time," Phys. Rev. Lett. **103**, 136001 (2009).

[14] Hawke, L. G. D., Q. Huang, O. Hassager, and D. J. Read, "Modifying the pom-pom model for extensional viscosity overshoots," J. Rheol. **59**, 995–1017 (2015).

[15] Ianniruberto, G., "Extensional flows of solutions of entangled polymers confirm reduction of friction coefficient," Macromolecules **48**, 6306–6312 (2015).

[16] Mead, D. W., N. Banerjee, and J. Park, "A constitutive model for entangled polymers incorporating binary entanglement pair dynamics and a configuration dependent friction coefficient," J. Rheol. **59**, 335–363 (2015).

[17] Mead, D. W., S. Monjezi, and J. Park, "A constitutive model for entangled polydisperse linear flexible polymers with entanglement dynamics

and a configuration dependent friction coefficient. Part II. Modeling "shear modification" following cessation of fast shear flows," J. Rheol. **62**, 135–147 (2018).

[18] Mead, D. W., S. Monjezi, and J. Park, "A constitutive model for entangled polydisperse linear flexible polymers with entanglement dynamics and a configuration dependent friction coefficient. Part I: Model derivation," J. Rheol. **62**, 121–134 (2018).

[19] Collis, M. W., A. K. Lele, M. R. Mackley, R. S. Graham, D. J. Groves, A. E. Likhtman, T. M. Nicholson, O. G. Harlen, T. C. B. McLeish, L. R. Hutchings, C. M. Fernyhough, and R. N. Young, "Constriction flows of monodisperse linear entangled polymers: Multiscale modeling and flow visualization," J. Rheol. **49**, 501–522 (2005).

[20] Dealy, J. M., and R. G. Larson, *Structure and Rheology of Molten Polymers—From Structure to Flow Behavior and Back Again* (Hanser, Munich, 2006).

[21] Boudara, V., Supramolecular and entangled polymer materials: Rheological models, Ph.D. thesis, University of Leeds, Leeds, 2017.

[22] Boudara, V. A. H., J. D. Peterson, L. G. Leal, and D. J. Read, "Nonlinear rheology of polydisperse blends of entangled linear polymers: Rolie-Double-Poly models," J. Rheol. **63**, 71–91 (2018).

[23] Read, D. J., M. E. Shivokhin, and A. E. Likhtman, "Contour length fluctuations and constraint release in entangled polymers: Slip-spring simulations and their implications for binary blend rheology," J. Rheol. **62**, 1017–1036 (2018).

[24] Viovy, J. L., M. Rubinstein, and R. H. Colby, "Constraint release in polymer melts: Tube reorganization versus tube dilation," Macromolecules **24**, 3587–3596 (1991).

[25] Read, D. J., K. Jagannathan, S. K. Sukumaran, and D. Auhl, "A full-chain constitutive model for bidisperse blends of linear polymers," J. Rheol. **56**, 823–873 (2012).

[26] Graham, R. S., J. Bent, L. R. Hutchings, R. W. Richards, D. J. Groves, J. Embery, T. M. Nicholson, T. C. B. McLeish, A. E. Likhtman, O. G. Harlen, D. J. Read, T. Gough, R. Spares, P. D. Coates, and I. Grillo, "Measuring and predicting the dynamics of linear monodisperse entangled polymers in rapid flow through an abrupt contraction. A small angle neutron scattering study," Macromolecules **39**, 2700–2709 (2006).

[27] Scelsi, L., M. R. Mackley, H. Klein, P. D. Olmsted, R. S. Graham, O. G. Harlen, and T. C. B. McLeish, "Experimental observations and matching viscoelastic specific work predictions of flow-induced crystallization for molten polyethylene within two flow geometries," J. Rheol. **53**, 859–876 (2009).

[28] Hassell, D. G., D. Hoyle, D. Auhl, O. Harlen, M. R. Mackley, and T. C. B. McLeish, "Effect of branching in cross-slot flow: The formation of "W cusps"," Rheol. Acta **48**, 551–561 (2009).

[29] Bishko, G., Implementing molecular rheology in complex flow fields: A Lagrangian simulation, University of Leeds, Leeds, 1997.

[30] Rolón-Garrido, V. H., M. H. Wagner, C. Luap, and T. Schweizer, "Modeling non-Gaussian extensibility effects in elongation of nearly monodisperse polystyrene melts," J. Rheol. **50**, 327–340 (2006).

[31] Marrucci, G., "Dynamics of entanglements: A nonlinear model consistent with the Cox-Merz rule," J. Nonnewton. Fluid **62**, 279–289 (1996).

[32] See supplementary material at https://doi.org/10.1122/1.5058207 for the monodisperse and polydisperse Rolie-Poly elements used throughout this work and the SER data for P627-S.